Fluid Dynamics and Viscosity in Strongly Correlated Fluids

Thomas Schäfer

Department of Physics, North Carolina State University, Raleigh, North Carolina 27695

Annu. Rev. Nucl. Part. Sci. 2014. 64:125–48

First published online as a Review in Advance on June 27, 2014

The *Annual Review of Nuclear and Particle Science* is online at nucl.annualreviews.org

This article's doi: 10.1146/annurev-nucl-102313-025439

Keywords

nonequilibrium physics, kinetic theory, holographic duality

Abstract

We review the modern view of fluid dynamics as an effective low-energy, long-wavelength theory of many-body systems at finite temperature. We introduce the concept of a nearly perfect fluid, defined by a ratio η/s of shear viscosity to entropy density of order $\hbar/k_B$ or less. Nearly perfect fluids exhibit hydrodynamic behavior at all distances down to the microscopic length scale of the fluid. We summarize arguments that suggest that there is fundamental limit to fluidity, and we review the current experimental situation of measurements of η/s in strongly coupled quantum fluids.

Contents

$\pi\alpha\nu\tau\alpha\ \rho\epsilon\iota$. (Everything flows.)

The mountains flowed before the Lord.
—Prophet Deborah, Judg. 5:5

1. FLUID DYNAMICS

1.1. Fluid Dynamics as an Effective Theory

Fluid dynamics is often described as a consequence of applying Newton's laws to a continuous deformable medium. However, the ideas underlying fluid dynamics are much more general. Fluid dynamics describes classical and quantum liquids, gases, and plasmas. It accounts for the low-energy properties of magnetic materials, liquid crystals, crystalline solids, supersolids, and many other systems. Indeed, fluid dynamics is now understood as an effective theory for the long-distance, long-time properties of any material (1, 2). The only requirement for the applicability of fluid dynamics is that the system relax to approximate local thermodynamic equilibrium on the timescale of the observation. This idea is captured by the two quotations above: In principle everything behaves as a fluid, but in some systems observing fluid dynamic behavior may require divine patience (3).

Fluid dynamics is based on the observation that there are two basic timescales associated with the behavior of a many-body system. The first is a microscopic timescale, $\tau_{\rm fluid}$, that characterizes the rate at which a generic disturbance relaxes. In a typical molecular liquid, this rate is governed by the collision rate between molecules. The second timescale, $\tau_{\rm diff}$, is associated with the relaxation of conserved charges. Because conserved charges cannot relax locally but rather have to decay

by diffusion or collective motion, this time increases with the length scale λ of the disturbance: $\tau_{\rm diff} \sim \lambda$. Fluid dynamics is based on the separation of scales $\tau_{\rm fluid} \ll \tau_{\rm diff}$, and $\omega_{\rm fluid} = \tau_{\rm fluid}^{-1}$ can be viewed as the breakdown scale of fluid dynamics as an effective theory.

In a simple nonrelativistic fluid, the conserved charges are the mass density ρ, the momentum density $\boldsymbol{\pi}$, and the energy density $\mathcal{E}$. The momentum density can be used to define the fluid velocity: $\boldsymbol{u} = \boldsymbol{\pi}/\rho$. By Galilean invariance, the energy density can then be written as the sum of the internal energy density and kinetic energy density: $\mathcal{E} = \mathcal{E}_0 + \frac{1}{2}\rho u^2$. The conservation laws are

$$\frac{\partial \rho}{\partial t} = -\boldsymbol{\nabla} \cdot \boldsymbol{\pi}, \qquad 1.$$

$$\frac{\partial \pi_i}{\partial t} = -\nabla_j \Pi_{ij}, \qquad 2.$$

$$\frac{\partial \mathcal{E}}{\partial t} = -\boldsymbol{\nabla} \cdot \boldsymbol{j}^{\epsilon}. \qquad 3.$$

For these equations to close, we have to specify constitutive relations for the stress tensor Π_{ij} and the energy current $\boldsymbol{j}^{\epsilon}$. Because fluid dynamics is an effective long-wavelength theory, we expect that the currents can be systematically expanded in gradients of the hydrodynamic variables ρ, $\boldsymbol{u}$, and $\mathcal{E}_0$. In the case of the stress tensor, the leading, no-derivative terms are completely fixed by rotational symmetry and Galilean invariance. We have

$$\Pi_{ij} = \rho u_i u_j + P\delta_{ij} + \delta\Pi_{ij}, \qquad 4.$$

where $P = P(\rho, \mathcal{E}_0)$ is the equation of state and $\delta\Pi_{ij}$ contains gradient terms. The approximation $\delta\Pi_{ij} = 0$ is known as ideal fluid dynamics. Ideal fluid dynamics is time reversal invariant and the entropy is conserved. If gradient terms are included, then time reversal invariance is broken and the entropy increases. We refer to $\delta\Pi_{ij}$ as the dissipative stresses. At first order in the gradient expansion, $\delta\Pi_{ij}$ can be written as $\delta\Pi_{ij} = -\eta\sigma_{ij} - \zeta\delta_{ij}\langle\sigma\rangle$, with

$$\sigma_{ij} = \nabla_i u_j + \nabla_j u_i - \frac{2}{3}\delta_{ij}\langle\sigma\rangle, \quad \langle\sigma\rangle = \boldsymbol{\nabla} \cdot \boldsymbol{u}. \qquad 5.$$

This expression contains two transport coefficients, the shear viscosity η and the bulk viscosity ζ. The energy current is given by $\boldsymbol{j}^{\epsilon} = \boldsymbol{u}w + \delta\boldsymbol{j}^{\epsilon}$, where $w = P + \mathcal{E}$ is the enthalpy. At leading order in the gradient expansion, $\delta j_i^{\epsilon} = u_j\delta\Pi_{ij} - \kappa\nabla_i T$, where κ is the thermal conductivity. The second law of thermodynamics implies that η, ζ, and κ must be positive.

We can now establish the expansion parameter that controls the fluid dynamic description. We first note that the ideal stress tensor contains two terms, which are related to the pressure P and the inertial stress $\rho u_i u_j$. The relative importance of these two terms is governed by the Mach number $\mathrm{Ma} = v/c_s$, where $c_s^2 = (\partial P)/(\partial\rho)_{\bar{s}}$ is the speed of sound and $\bar{s} = s/n$ is the entropy per particle. Flows with $\mathrm{Ma} \sim 1$ are termed compressible, and flows with $\mathrm{Ma} \ll 1$ incompressible. We are most interested in expanding systems, which are certainly compressible.

The validity of hydrodynamics requires that dissipative terms be small relative to ideal terms. We focus on the role of shear viscosity both because it is the dominant source of dissipation in the systems considered here and because both ζ and κ can become zero in physically realizable limits. In particular, ζ vanishes in a scale-invariant fluid such as the unitary gas, and κ vanishes in a relativistic fluid with zero baryon chemical potential such as the pure gluon plasma. In the case in which $\mathrm{Ma} \sim 1$, the expansion parameter is

$$\mathrm{Re}^{-1} = \frac{\eta\nabla u}{\rho u^2} = \frac{\eta}{\rho u L}, \qquad 6.$$

where Re is the Reynolds number and L is a characteristic length scale of the flow. Before continuing, we briefly comment on incompressible flows. The expansion parameter in this case is $\mathrm{Ma}^2/\mathrm{Re}$. Flows with $\mathrm{Ma} \ll 1$ and $\mathrm{Re}^{-1} \ll 1$ are nearly ideal, turbulent flows. The regime in which $\mathrm{Ma}^2/\mathrm{Re} \ll 1$ but $\mathrm{Re}^{-1} \gtrsim 1$ is that of very viscous flow. Today, interest in very viscous flow is often related to classical fluids in confined geometries. A typical example is the problem of bacterial swimming (4).

We note that Re^{-1} can be written as

$$\mathrm{Re}^{-1} = \frac{\eta}{\hbar n} \times \frac{\hbar}{muL}, \qquad 7.$$

where both factors are dimensionless. The first factor is solely a property of the fluid, and the second factor characterizes the flow. For a typical classical flow, the second factor is much smaller than one, and the validity of fluid dynamics places no constraints on $\eta/(\hbar n)$. For the types of experiments that are explored in Sections 2 and 3, the second factor is of order one and the applicability of fluid dynamics requires $\eta \lesssim \hbar n$. We note that in relativistic flows the inertial term is $\Pi_{ij} = sTu_iu_j$ and the analogous requirement is $\eta \lesssim \hbar s/\mathrm{k_B}$. We refer to fluids that satisfy this condition as nearly perfect fluids (5–8) and show that these fluids exhibit hydrodynamic behavior on remarkably short length and timescales, comparable to microscopic scales such as the inverse temperature or the inverse Fermi wave vector. Throughout this review, we use units in which $\hbar = \mathrm{k_B} = 1$.

The long-wavelength expansion can be extended beyond the first order in gradients of the hydrodynamic variables. The classical higher-order equations are known as Burnett and super-Burnett equations (9, 10). Explicit forms of second-order terms based on kinetic theory were derived by Grad (11) in the nonrelativistic case, as well as by Israel & Stewart (12) and others for relativistic fluids. Historically, these theories have not been used very frequently. One reason is that the effects are not very large. In the case of the Navier–Stokes equation, dissipative terms can exponentiate and alter the motion qualitatively, even if at any given time gradient corrections are small. A simple example is a collective oscillation of a fluid (see Section 2.2). Without viscosity the mode cannot decay, but if dissipation is present the motion is exponentially damped. Typically, second-order terms do not exponentiate, and the gain in accuracy from including higher-order terms is frequently offset by uncertainties in higher-order transport coefficients or the need for additional boundary conditions.

The second reason that these theories are infrequently used is that the classical equations at second order are unstable to short-wavelength perturbations. In relativistic fluid dynamics, problems with acausality and instability already appear at the Navier–Stokes level. These difficulties are not fundamental: Fluid dynamics is an effective theory, and unstable or acausal modes occur outside the domain of validity of the theory. It is nevertheless desirable to construct schemes that have second- or higher-order accuracy and satisfy causality and stability requirements. A possible solution is to promote the dissipative currents to hydrodynamic variables and postulate a set of relaxation equations for these quantities. Consider the dissipative stress tensor and define $\pi_{ij} = \delta\Pi_{ij}$. The relaxation equation for π_{ij} is

$$\tau_\mathrm{R}\dot{\pi}_{ij} = -\pi_{ij} - \eta\sigma_{ij} + \ldots, \qquad 8.$$

where the ellipse contains second-order terms such as $(\nabla \cdot u)\sigma_{ij}$ and $\sigma_{ik}\sigma_{kj}$. To second-order accuracy, this equation is equivalent to $\delta\Pi_{ij} = -\eta\sigma_{ij} + \tau_\mathrm{R}\eta\dot{\sigma}_{ij} + \ldots$, which is part of standard Burnett theory. Physically, Equation 8 describes the relaxation of the dissipative stresses to the Navier–Stokes form. The resulting equations are stable and causal, and the sensitivity to higher-order gradients can be checked by varying second-order coefficients such as τ_R (13).

Equation 8 was first proposed by Maxwell as a model for very viscous fluids. Cattaneo (14) observed that relaxation equations can be used to restore causality and studied a relaxation model in the context of Fourier's law, $\delta \boldsymbol{j}^{\epsilon} = -\kappa \nabla T$ (15). Relaxation equations were derived from kinetic theory by Müller (16), Israel & Stewart (17), and others. To achieve the expected scaling of second-order terms with Re^{-2} it is important to include a full set of second-order terms that respect the symmetries of the theory. This problem was addressed for relativistic scale-invariant fluids by Baier et al. (18) and in the nonrelativistic case by Chao & Schäfer (19).

It is well known that the low-energy expansion in effective field theories is not a simple power series in the expansion parameter ω/Λ. Quantum fluctuations lead to nonanalytic terms. In the case of fluid dynamics, $\Lambda = \omega_{\mathrm{fluid}}$ and nonanalyticities arise due to thermal fluctuations of the hydrodynamic variables. As a consequence, the dissipative currents $\delta\Pi_{ij}$ and $\delta \boldsymbol{j}^{\epsilon}$ contain not only gradient terms but also stochastic contributions. The magnitude of the stochastic terms is determined by fluctuation-dissipation theorems. We have

$$\left\langle \Pi_{ij}(t,\boldsymbol{x})\Pi_{kl}(t',\boldsymbol{x}')\right\rangle = 2\eta T\left(\delta_{ik}\delta_{jl}+\delta_{il}\delta_{jk}-\frac{2}{3}\delta_{ij}\delta_{kl}\right)\delta(t-t')\delta(\boldsymbol{x}-\boldsymbol{x}'), \qquad 9.$$

$$\left\langle j_i^{\epsilon}(t,\boldsymbol{x})j_j^{\epsilon}(t',\boldsymbol{x}')\right\rangle = 2\kappa T^2\delta_{ij}\delta(t-t')\delta(\boldsymbol{x}-\boldsymbol{x}'), \qquad 10.$$

where $\langle . \rangle$ denotes a thermal average and we have neglected bulk viscosity. A calculation of the response function in stochastic fluid dynamics shows that the hydrodynamic expansion contains nonanalyticities that are smaller than the Navier–Stokes term but larger than second-order terms (20, 21). This finding implies that, strictly speaking, the second-order theory is consistent only if stochastic terms are included. Some studies of fluctuating fluid dynamics have been performed (22), but in particle and nuclear physics this problem has only recently attracted interest (23).

1.2. Microscopic Models of Fluids: Kinetic Theory

Within fluid dynamics, the equation of state and the transport coefficients are parameters that have to be extracted from experiments. If a more microscopic description of the fluid is available, then we can compute these parameters in terms of more fundamental quantities. The simplest microscopic description of a fluid is kinetic theory. Kinetic theory is itself an effective theory that describes the long-distance behavior of an underlying classical or quantum many-body system. It is applicable whenever there is a range of energies and momenta in which the excitations of the fluid are long-lived quasi-particles. Kinetic theory can be used to relate properties of these quasi-particles—their masses, lifetimes, and scattering cross sections—to the equation of state and the transport coefficients. Kinetic theory can also be used to extend the description of collective effects, such as sound or macroscopic flow, into the regime where fluid dynamics breaks down.

The basic object in kinetic theory is the quasi-particle distribution function $f_p(\boldsymbol{x},t)$. Hydrodynamic variables can be written as integrals of f_p over $\mathrm{d}\Gamma = \mathrm{d}^3 p/(2\pi)^3$. For example, the off-diagonal component of the stress tensor is given by

$$\Pi_{ij}(\boldsymbol{x},t) = \int \mathrm{d}\Gamma_p\, p_i v_j f_p(\boldsymbol{x},t), \quad (i\neq j), \qquad 11.$$

where $\boldsymbol{v} = \nabla_p E_p$ is the quasi-particle velocity. Similar expressions exist for other conserved currents. The equation of motion for $f_p(\boldsymbol{x},t)$ is the Boltzmann equation,

$$\left(\frac{\partial}{\partial t}+\boldsymbol{v}\cdot\nabla_x+\boldsymbol{F}\cdot\nabla_p\right) f_p(\boldsymbol{x},t) = C[f_p], \qquad 12.$$

where $\boldsymbol{F} = -\boldsymbol{\nabla}_x E_p$ is the force and $C[f_p]$ is the collision term. By taking moments of the Boltzmann equation, we can derive the conservation laws (1–3). To extract the constitutive relations, we have to assume that the distribution function is close to the equilibrium distribution, $f_p(\boldsymbol{x}) = f_p^0(\boldsymbol{x}) + \delta f_p(\boldsymbol{x})$, and that the spatial variation of $f_p(x)$ is small. The equilibrium distribution can be expressed in terms of the conserved charges or, more conveniently, in terms of the corresponding intensive quantities μ, T, and $\boldsymbol{u}$. We find

$$f_p^0(\boldsymbol{x}) = \frac{1}{\exp[\beta(E_p - \boldsymbol{u}\cdot\boldsymbol{p} - \mu)] \pm 1}, \qquad 13.$$

where $\beta = 1/T$; the plus/minus sign corresponds to fermions/bosons, respectively; and β, μ, and $\boldsymbol{u}$ are functions of $\boldsymbol{x}$ and t.

To identify the expansion parameter, we have to understand the scales involved in the collision term. If $\delta f_p \ll f_p^0$, we can use $C[f_p^0] = 0$ to linearize the collision term. The linearized collision term is a Hermitian, negative semidefinite operator that can be expanded in terms of its eigenvalues and eigenvectors. We refer to the inverse eigenvalues as collision times. At long times, we can approximate the collision term by the longest collision time τ_0 and write

$$C[f_p^0 + \delta f_p] \simeq -\frac{\delta f_p}{\tau_0}, \qquad 14.$$

where we have used the fact that at late times δf_p is dominated by its projection on the lowest eigenvector. Equation 14 is known as the Bhatnagar–Gross–Krook (BGK) or relaxation time approximation (24). We can define a mean free path by $l_{\rm mfp} = \tau_0 \bar{v}$, where $\bar{v} = \langle v^2 \rangle^{1/2}$. The expansion parameter for the gradient expansion is given by the Knudsen number,

$$\mathrm{Kn} = \frac{l_{\rm mfp}}{L}, \qquad 15.$$

where $L \sim \nabla^{-1}$, as in Equation 6. The systematic determination of the constitutive equation via an expansion in Kn is termed the Chapman–Enskog expansion (25). We find, for example,

$$\eta = \frac{1}{3} n l_{\rm mfp} \bar{p}, \qquad 16.$$

and $\tau_{\rm R} = \tau_0 = \eta/P$ (19, 25). To estimate the Reynolds number, we can use $\mathrm{Ma} = u/c_s \sim 1$. In kinetic theory we find $c_s^2 = \frac{5}{9}\langle v^2 \rangle$ and $\mathrm{Kn} \sim \mathrm{Re}^{-1}$. The Knudsen expansion is equivalent to the Reynolds number expansion in fluid dynamics.

Fluid dynamics corresponds to the long-time behavior of kinetic theory. It is also interesting to examine the short-time behavior. Consider the response of the fluid to an external shear strain h_{xy} with frequency ω and wave number k. The solution of the Boltzmann equation is of the form

$$\delta f_p(\omega, k) = \frac{1}{2T} \frac{-i\omega p_x v_y}{-i\omega + i\boldsymbol{v}\cdot\boldsymbol{k} + \tau_0^{-1}} f_p^0 h_{xy}. \qquad 17.$$

This result can be used to compute the spectral function of correlators of conserved currents. For $k = 0$, the term $(-i\omega + \tau_0^{-1})$ in the denominator of Equation 17 leads to a Lorentzian shape of the spectral function, which is a signature of the presence of quasi-particles. The spectral function also provides information about the breakdown of kinetic theory for large ω and k. There is no intrinsic scale in the Boltzmann equation other than the collision time τ_0, which sets the scale for the hydrodynamic expansion. The high-energy scale is set by matching the Boltzmann equation to the equation of motion for a nonequilibrium Green function in quantum field theory (26). Instead of matching these equations explicitly, we can compare the kinetic spectral functions in Equation 17 with the spectral functions in quantum field theory (see Section 2.1). The result is that the breakdown scale is $\omega_{\rm micro} \sim T$. This result should be compared with the hydrodynamic

scale, $\omega_{\rm fluid} \sim \tau_0^{-1} \sim P/\eta$. For a typical fluid these scales are well separated, but for a nearly perfect fluid the two scales are comparable. At least parametrically, in a nearly perfect fluid there is no room for kinetic theory; that means there is no regime in which kinetic theory is more accurate than fluid dynamics.

The collision term is determined by the quasi-particle cross section σ, and a rough estimate of the mean free path is given by $l_{\rm mfp} = 1/(n\sigma)$. Using Equation 16, we find $\eta \sim \bar{p}/\sigma$. This result has two interesting consequences:

1. The viscosity of a dilute gas is independent of its density. The physical reason for this behavior is that viscosity is determined by the rate of momentum diffusion. The number of particles is proportional to n, but the mean free path scales as $1/n$. As a result, the diffusion rate is constant. Maxwell was so surprised by this result that he tested it by measuring the damping rate of a torsion pendulum in a sealed container as a function of the air pressure (27, 28). He confirmed that η is not a function of P at fixed T. Of course, if the air is very dilute, then $l_{\rm mfp} > L$ and the hydrodynamic description breaks down. In this limit, known as the Knudsen regime, damping is proportional to pressure.
2. The result $\eta \sim 1/\sigma$ also implies that viscosity of a weakly coupled gas is very large, which is counterintuitive because we think of viscosity as friction between fluid layers. Consider a fluid sheared between two parallel plates in the xz plane. The force per unit area is

$$\frac{F}{A} = \eta \nabla_y u_x. \tag{18.}$$

We naïvely expect this force to grow with the strength of the interaction. Our intuition is shaped by very viscous fluids, for which viscosity is indeed determined by force chains and solid friction. This expectation is not entirely inappropriate, because the word viscosity is derived from the Latin name for mistletoe, *Viscum album*.

1.3. Matching and Kubo Relations

In the case of kinetic theory, we can derive the equations of fluid dynamics from the underlying microscopic theory. In more complicated cases, for example, if the short-distance description is a strongly coupled field theory, this may not be possible. In that case, we can rely on the fact that fluid dynamics is a general long-distance effective theory, and compute the transport coefficients on the basis of the idea of matching. Matching expresses the requirement that in the regime of validity of the effective theory, correlation functions must agree with correlators in the microscopic theory. Consider the retarded correlation function of the stress tensor

$$G_{\rm R}^{xyxy}(\omega, \mathbf{k}) = -i \int {\rm d}t \int {\rm d}^3x \, e^{i\omega t - i\boldsymbol{k}\cdot\boldsymbol{x}} \Theta(t) \langle [\Pi^{xy}(t, \boldsymbol{x}), \Pi^{xy}(0, 0)] \rangle. \tag{19.}$$

In linear response theory, this function controls the stress induced by an external strain. In fluid dynamics, $\Pi_{xy} \simeq \rho u_x u_y$, and we can compute the correlation function from linearized hydrodynamics and fluctuation relations. We find

$$G_{\rm R}^{xyxy}(\omega, k) = P - i\eta\omega + \tau_{\rm R}\eta\omega^2 - \frac{\kappa_{\rm R}}{2}k^2 + O(\omega^3, \omega k^2), \tag{20.}$$

where $\tau_{\rm R}$ is the relaxation time defined in Equation 8 and $\kappa_{\rm R}$ is another second-order transport coefficient (21). Equation 20 implies the Kubo relation:

$$\eta = -\lim_{\omega\to 0} \lim_{k\to 0} \frac{\rm d}{{\rm d}\omega} {\rm Im} G_{\rm R}^{xyxy}(\omega, \boldsymbol{k}). \tag{21.}$$

This equation can be applied to field theory on the basis of Equation 19 and the microscopic definition of the stress tensor. This method is used to compute transport coefficients on the lattice in both relativistic and nonrelativistic field theories (29–34). The difficulty with using Kubo's formula is that imaginary-time Monte Carlo simulations do not provide direct access to correlation functions for real frequencies. Measuring the shear viscosity requires analytic continuation of imaginary-time data, which leads to uncertainties that are difficult to quantify. We note that some transport coefficients, such as the parameter κ_R in Equation 20, can be measured directly from imaginary-time data.

Equation 20 confirms that the expansion parameter of the hydrodynamic expansion is $\omega/\omega_{\rm fluid}$, where $\omega_{\rm fluid} \simeq P/\eta \simeq \tau_R^{-1}$. Note that fluctuations introduce nonanalytic terms at order $\omega^{3/2}$ (20, 21). This is a breakdown of the gradient expansion but not a breakdown of hydrodynamics. For example, at second order in the low-energy expansion, the $\omega^{3/2}$ term is completely determined by η and P, and the relaxation time τ_R can be extracted by matching $G_R(\omega)$ to the low-energy expansion in fluid dynamics.

1.4. Microscopic Models of Fluids: Holography

Kinetic theory provides explicit theoretical realizations of weakly coupled fluids. Holographic dualities and the anti–de Sitter/conformal field theory (AdS/CFT) correspondence have led to controlled realizations of strongly coupled fluids. The basic idea originated from the study of black holes. It has been known for some time that black holes have entropy and that the process of a perturbed black hole settling down into a stationary configuration bears some resemblance to dissipative relaxation in fluids. Indeed, one can assign shear viscosity and electric conductivity to the "stretched horizon," an imaginary surface that hovers just above the event horizon (35).

These ideas were made precise in the context of the AdS/CFT correspondence (36; see References 37–40 for reviews). In the simplest case, consider a Schwarzschild black hole embedded in five-dimensional AdS (AdS_5) space. The full space-time has additional compact dimensions, which are required by string theory but play no role in our discussion. Black holes in AdS_5 do not evaporate, and the black hole is in thermal equilibrium. This means that the rate of Hawking radiation balances the amount of energy falling back into the black hole. On the basis of its causal structure, we can view AdS_5 as having a "boundary," which is four-dimensional Minkowski space. Matter on the boundary is in thermal equilibrium with the black hole space-time.

The AdS/CFT correspondence asserts that the boundary is described by an ordinary quantum field theory and that the correlation functions of this field theory have a dual description in terms of boundary correlation functions of a gravitational theory in the bulk. The correspondence is simplest if the boundary theory is strongly coupled and contains a large number N degrees of freedom. In this case, the bulk theory is simply classical gravity. The partition function of the boundary quantum field theory is

$$Z_{\rm QFT}[J_i] = \exp(-S[\phi_i|_{\partial M} = J_i]), \qquad 22.$$

where J_i is a set of sources in the field theory, S is the gravitational action, ϕ_i is a dual set of fields in the gravitational theory, and ∂M is the boundary of AdS_5. The fields ϕ_i satisfy classical equations of motions subject to boundary conditions on ∂M.

The original construction involves a black hole in AdS_5 and is dual to a relativistic fluid governed by a generalization of QCD known as $\mathcal{N} = 4$ super-Yang–Mills theory. This theory is considered in the limit of a large number of colors N_c. The gravitational theory is Einstein gravity with

additional matter fields that are not relevant here. The AdS_5 black hole metric is

$$ds^2 = \frac{(\pi TR)^2}{u}[-f(u)dt^2 + d\boldsymbol{x}^2] + \frac{R^2}{4u^2 f(u)}du^2, \qquad 23.$$

where $\boldsymbol{x}$ and t are Minkowski space coordinates and u is a "radial" coordinate, where $u = 1$ is the location of the black hole horizon and $u = 0$ is the boundary. T is the temperature, R is the AdS radius, and $f(u) = 1 - u^2$. In the boundary theory, the metric couples to the stress tensor $\Pi_{\mu\nu}$. Correlation functions of the stress tensor can be found by linearizing the bulk action around the AdS_5 solution, $g_{AB} = g^0_{AB} + \delta g_{AB}$, where $A, B = 1, \ldots, 5$. Small oscillations of the off-diagonal strain δg^y_x are particularly simple. We consider harmonic dependence on the Minkowski coordinates $\delta g^y_x = \phi_p(u)e^{ikx - i\omega t}$. Fluctuations are governed by the wave equation

$$\phi_p''(u) - \frac{1+u^2}{uf(u)}\phi_p'(u) + \frac{\omega^2 - k^2 f}{(2\pi T)^2 u f(u)^2}\phi_p(u) = 0. \qquad 24.$$

This differential equation has two linearly independent solutions. The retarded correlation function corresponds to picking a solution that is purely infalling at the horizon (37). For small (or very large) ω and k, this solution can be found analytically (41, 42). $G_R(\omega, k)$ is computed by inserting the solution into the Einstein–Hilbert action, and then computing the variation with respect to the boundary value of δg^y_x. The result is of the form given in Equation 20, with (18, 43)

$$P = \frac{sT}{4}, \quad \eta = \frac{s}{4\pi}, \quad \tau_R = \frac{2 - \log(2)}{2\pi T}. \qquad 25.$$

Note that in the case of a relativistic fluid, η is naturally expressed in units of the entropy density s, not the density n, because a relativistic fluid need not have a conserved particle number. As a rough comparison, we can use the fact that for a weakly interacting relativistic gas $s/n = 3.6$. We observe that the AdS/CFT correspondence describes a very good fluid. In particular, $\eta/s < 1$ and $\tau_R \sim T^{-1}$. This is a remarkable result because the AdS/CFT correspondence has provided the first reliable theoretical description of a nearly perfect fluid.

Many aspects of the strongly coupled fluid can be studied using AdS/CFT:

1. The spectral function $\eta(\omega) = -\frac{1}{\omega}\mathrm{Im}G_R(\omega)$ does not show evidence for quasi-particles (42, 44). Instead of a Lorentzian of width $1/\tau_R$, one finds a smooth function that interpolates between the hydrodynamic limit $\eta(0) = \eta$ and the high-frequency limit $\eta(\omega) \sim \omega^3$. Because of nonrenormalization theorems, the $\omega \to \infty$ limit is given by the correlation function in free field theory.
2. The relaxation time can written as $\tau_R = c\,\eta/P$, where $c = [2 - \log(2)]/2 \simeq 0.65$. This value can be compared with the Israel–Stewart result, $\tau_R = 1.5\,\eta/P$. We observe that the relaxation time is very short, but in units of η/P it is only a factor of 2.3 smaller than kinetic theory would predict. The AdS/CFT correspondence has also been used to compute other second-order transport coefficients (18).
3. The validity of the hydrodynamic expansion is controlled by the location of the poles of $G_R(\omega)$ in the complex ω plane. The hydrodynamic pole of the shear correlator is located at $\omega \simeq i D_\eta k^2$, where $D_\eta = \eta/(sT)$ is the momentum diffusion constant. Nonhydrodynamic poles correspond to so-called quasi-normal modes of the linearized Einstein equations. These quasi-normal modes come in complex conjugate pairs and are located at a minimum distance of order T from the real axis (45). This observation confirms that the expansion parameter in a nearly perfect fluid is ω/T.
4. Using the AdS/CFT correspondence, one can study the approach to equilibrium in great detail. For initial conditions that lead to Bjorken flows, the approach to hydrodynamics is very rapid. After the quasi-normal modes are damped, on timescales on the order of $(\tau T) \lesssim 1$,

the Navier–Stokes description is very accurate, even though nonequilibrium contributions to the pressure can be large (46, 47). This phenomenon is sometimes referred to as rapid hydrodynamization.

5. Heller et al. (48) studied the large-order behavior of the hydrodynamic expansion for a Bjorken-like flow. They found that the gradient expansion is an asymptotic series and that the radius of convergence is zero. The coefficients of high-order terms, and the leading singularity in the Borel plane, are governed by the lowest quasi-normal mode. We note that this phenomenon is unrelated to the nonanalytic terms in the expansion mentioned above. The calculation is performed in the large-N_c limit of the field theory, so nonanalytic terms in the gradient expansion are suppressed (49). Heller et al. speculate that the large-order behavior is analogous to the factorial divergence of large orders of perturbation theory in quantum field theory.

Finally, we note that one can directly derive the equation of fluid dynamics by promoting the parameters that label the near horizon metric to hydrodynamic variables (50). Solving the resulting Einstein equations order by order in gradients provides an alternative derivation of the second-order transport coefficients discussed above. This method provides a general connection between solutions of the Einstein equation and the Navier–Stokes equation, referred to as the fluid–gravity correspondence (51).

1.5. Viscosity Bounds

The AdS/CFT correspondence provides an explicit, albeit somewhat theoretical, example of a nearly perfect fluid, leading to two questions: Can nearly perfect fluids be realized in the laboratory, and is there a fundamental limit to fluidity? We address the first question in Sections 2 and 3 below. There are several arguments that the answer to the second question is affirmative. We summarize these arguments here.

1.5.1. Uncertainty relation. Kinetic theory predicts that $\eta = \frac{1}{3} n l_{\rm mpf} \bar{p}$ and that low viscosity corresponds to a short mean free path (5). However, the uncertainty relation suggests that the product of the mean free path and mean momentum cannot become arbitrarily small. Using $l_{\rm mpf} \bar{p} \gtrsim 1$ implies $\eta/n \gtrsim 1/3$. This argument was originally presented in the context of relativistic fluids. In these systems, the inverse Reynolds number is given by $\eta/(s\tau T)$. Using the entropy per particle of a weakly interacting relativistic Bose gas, $s/n = 3.6$, we get $\eta/s \gtrsim 0.09$.

There are several issues with this argument. First, it is based on the application of kinetic theory in a regime where there are no well-defined quasi-particles and the theory is not applicable. Second, there is no obvious reason that the entropy per particle cannot be much larger than the free-gas value (52). Finally, a bound on transport coefficients related to the uncertainty relation was first proposed by Mott (53) in connection with electric conductivity. A minimal conductivity implies that the metal–insulator transition must be continuous. However, this prediction is known to be false. Continuous metal–insulator transitions have been observed (54), and the physical mechanism of these transitions can be understood in terms of Anderson localization.

1.5.2. Holographic dualities. The value $\eta/s = 1/(4\pi)$ is obtained in the strong coupling limit of a large class of holographic theories (6). These theories are characterized by the fact that the dual gravitational description involves the Einstein–Hilbert action (37, 55, 56). Kovtun, Son, and Starinets (KSS) conjectured that the strong coupling result is an absolute lower bound for the ratio η/s in all fluids,

$$\frac{\eta}{s} \geq \frac{1}{4\pi}. \qquad 26.$$

This idea is a significant step forward compared with the argument based on the uncertainty relation. The value $1/(4\pi)$ is the result of a reliable calculation. Holographic dualities explain why the relevant quantity is η/s, and they account for the difference between momentum and charge diffusion. The diffusion constant goes to zero in the strong coupling limit (57–59), whereas the ratio η/s remains finite.

However, holographic theories exist that provide counterexamples to the KSS conjecture (60, 61). Finite coupling corrections increase the ratio η/s, but there are cases in which calculable finite N_c corrections decrease η/s. In terms of the dual description, these theories correspond to gravitational theories that contain a certain higher-derivative correction to the Einstein–Hilbert action, known as the Gauss–Bonnet term (62). Although this result rules out the KSS conjecture, there are compelling arguments for a weaker version of the viscosity bound. Given that the violation of the KSS bound can be related to the Gauss–Bonnet term, one has to study constraints on the Gauss–Bonnet coefficient λ_{GB}. It was found that high values of λ_{GB} lead to violations of causality. For the class of theories that are known to violate the KSS bound, causality implies the slightly weaker bound $\eta/s \geq (16/25)(1/4\pi)$ (63). It seems likely that this is not the final word from holographic dualities. Generalizations of Gauss–Bonnet gravity, so-called Lovelock theories, have been studied (64), and lower values of η/s may be possible.

1.5.3. Fluctuations. Shear viscosity is related to momentum diffusion, and $\eta/s = 0$ implies that mean free path for momentum transport is zero (20, 21). However, in fluid dynamics momentum can also be carried by collective modes such as sound and shear waves. Indeed, if the viscosity is small, this process becomes more efficient because the damping rate of sound and shear modes is small. This observation suggests that the physical viscosity of the fluid cannot be zero.

This argument can be made more precise using the low-energy expansion of hydrodynamic correlation functions. Fluctuations not only contribute to nonanalytic terms in $G_R(\omega)$, but also correct the polynomial terms that determine the transport coefficients. The retarded shear stress correlator in a relativistic fluid is of the form $G_R(\omega) = P + \delta P + i\omega(\eta + \delta\eta) + \ldots$, where δP is a correction to the pressure and

$$\eta + \delta\eta = \eta + \frac{17}{120\pi^2}\frac{\Lambda_K D_\eta s^2 T^3}{\eta^2} \qquad 27.$$

is the physical viscosity. Here, Λ_K is the breakdown momentum of the hydrodynamic description and $D_\eta = \eta/(sT)$ is the momentum diffusion constant. The gradient expansion requires $\Lambda_K D_\eta \lesssim 1$. We observe that $\delta\eta \sim 1/\eta^2$, so the physical viscosity cannot become arbitrarily small. The bound for η/s depends on the equation of state. For a quark–gluon plasma (QGP) $\eta/s \gtrsim 0.1$ (20), and in a nonrelativistic Fermi gas $\eta/s \gtrsim 0.2$ (21).

The bound is interesting because it sheds some light on what is special about shear viscosity. The stress tensor is quadratic in the fluid velocity and has a leading-order, nonlinear coupling to shear waves. Other currents do not have nonlinear-mode couplings at leading order. The bound is not universal, but it is complementary to the holographic bounds in the sense that it operates only at finite N, whereas the holographic bounds are rigorous at infinite N.

It is difficult to summarize the situation regarding the proposed viscosity bounds. There is strong evidence that viscosity is different from other transport coefficients. We can find systems for which bulk viscosity, conductivity, or diffusion constants vanish, but physical effects, the universality of the graviton coupling in holographic theories, and the universality of the stress tensor in stochastic fluid dynamics make it difficult to find scenarios in which the shear viscosity vanishes. The precise value of the bound is not known, but empirically the value $\eta/s = 1/(4\pi)$ found in

simple holographic theories is a good approximation for the viscosity of the best quantum fluids that can be studied in the laboratory (as discussed further below).

2. NONRELATIVISTIC FLUIDS

2.1. The Unitary Fermi Gas

In the following two sections, we describe theoretical and experimental results regarding the transport properties of the two best fluids that have been studied in the laboratory (7). These two fluids are ultracold atomic Fermi gases magnetically tuned to a Feshbach resonance and the QGP produced in relativistic heavy-ion collisions at the Relativistic Heavy-Ion Collider (RHIC) in Brookhaven, New York, and the Large Hadron Collider (LHC) at CERN in Geneva, Switzerland.

Ultracold Fermi gases are composed of atoms with half-integer total spin. Experiments focus on alkali atoms such as ^{6}Li. These atoms can be confined in all-optical or magneto-optical traps. We concentrate on systems in which two hyperfine states are macroscopically occupied. Because the density and temperature are very low, details of the atomic interaction and the atomic structure are not resolved; each atom can be described as the two components of a pointlike nonrelativistic spin-1/2 fermion. The fermions are governed by the effective Lagrangian

$$\mathcal{L} = \psi^\dagger \left(i\partial_0 + \frac{\nabla^2}{2m} \right) \psi - \frac{C_0}{2} \left(\psi^\dagger \psi \right)^2 . \qquad 28.$$

The coupling constant C_0 is related to the s-wave scattering length a. At low temperature and density, neither higher partial waves nor range corrections are important. The two-body s-wave scattering matrix is

$$\mathcal{M} = \frac{4\pi}{m} \frac{1}{1/a + iq}, \qquad 29.$$

where q is the relative momentum. The precise relation between C_0 and a depends on the regularization scheme. In dimensional regularization, $C_0 = 4\pi a/m$. In the limit of weak coupling, this result follows from the Born approximation.

Of particular interest is the "unitarity" limit $a \to \infty$. In this limit, the system has no dimensionful parameters and the theory is scale invariant (65). The scattering amplitude behaves as $1/(iq)$, which saturates the s-wave unitarity bound. The two-body wave function scales as $1/r$, and the many-body system is strongly correlated even if the density is low. Experimentally, the unitarity limit can be studied using magnetically tuned Feshbach resonances (66, 67).

We note that even at unitarity the dilute Fermi gas has well-defined quasi-particles if the temperature is large. The average scattering amplitude scales as $\sigma \sim \langle q^{-2} \rangle \sim \lambda_{dB}^2$, where $\lambda_{dB} \sim (mT)^{-1/2}$ is the thermal wavelength. In the high-temperature limit the average cross section is small, and the collisional width of a fermion quasi-particle is $\Gamma \sim zT$ (68), where $z = (n\lambda^3)/2 \ll 1$ is the fugacity. In this regime the shear viscosity can be computed using kinetic theory. The result is (69, 70)

$$\eta = \frac{15}{32\sqrt{\pi}} (mT)^{3/2}. \qquad 30.$$

As expected, the viscosity is independent of density and increases with temperature. The ratio η/n scales as $1/z$ and is parametrically large. We also find $\eta/s \sim 1/[z \log(1/z)]$.

In the regime $z \gtrsim 1$, the unitary gas is strongly coupled. At $z \sim 12$, the system undergoes a phase transition to a superfluid (71). In the superfluid phase the $U(1)$ symmetry of the effective Lagrangian (Equation 28) is spontaneously broken, and at low temperature there is a well-defined

bosonic quasi-particle related to the $U(1)$ Goldstone mode. Momentum diffusion due to Goldstone modes can be studied using kinetic theory, and we find $\eta \sim T^{-5}$ (72). Combined with Equation 30, this result indicates that the viscosity has a minimum in the vicinity of the critical temperature. In this regime, there are no reliable calculations of transport properties, but T-matrix calculations suggest that η/n reaches a value of ~0.5 (73). We note that at T_c the entropy per particle is very close to one. Lower values of the shear viscosity, $\eta/s \simeq 0.2$, have been found in quantum Monte Carlo calculations (34).

In kinetic theory, the viscosity spectral function has a Lorentzian line shape with width $\tau_R^{-1} = P/\eta$ (74). In the strongly coupled regime, the shape of the spectral function is not known, but one can determine the asymptotic behavior for $\omega \to \infty$ as well as the frequency sum rule. The sum rule is given by (73, 75)

$$\frac{2}{\pi}\int d\omega \left[\eta(\omega) - \frac{\mathcal{C}}{15\pi\sqrt{m\omega}}\right] = \frac{2}{3}\mathcal{E}, \qquad 31.$$

where $\mathcal{C}$ is a short-distance coefficient known as the contact density, which measures the strength of short-range correlations (76), and the subtraction term inside the integral corresponds to the high-frequency tail of the spectral function (77). In the high-temperature limit, $\mathcal{C} = 4\pi n^2 \lambda_{dB}^2$, and one can check that the high-frequency tail smoothly matches kinetic theory for $\omega \sim T$. We can now identify the relevant scales that limit the fluid dynamic and kinetic descriptions: $\omega_{\text{fluid}} \sim zT$ and $\omega_{\text{micro}} \sim T$. For $z \ll 1$ we find the expected hierarchy of scales, but in the strongly correlated regime both scales are comparable.

2.2. Flow and Viscosity

Fluid dynamics can be observed in experiments that involve releasing the gas from a deformed trap. In typical experiments, the trap corresponds to a harmonic confinement potential, $V = (1/2)m(\omega_\perp^2 x_\perp^2 + \omega_z^2 z^2)$, with an aspect ratio $\omega_\perp/\omega_z \sim$ (20–30). In hydrostatic equilibrium, pressure gradients along the transverse direction are much larger than pressure gradients along the longitudinal direction. Hydrodynamic evolution after the gas is released converts this difference into different expansion velocities, and during the late stages of evolution the cloud is elongated along the transverse direction (**Figure 1**). The observation of this effect led to the discovery of nearly perfect fluidity in ultracold gases (78). Shear viscosity counteracts the differential acceleration and leads to a less deformed final state. The shear viscosity can be measured by studying the time evolution of the cloud radii (79, 80).

An alternative approach is based on recapturing the gas after release from the trap, which excites a transverse breathing mode. Hydrodynamic behavior can be verified by measuring the frequency of the collective mode. In an ideal fluid, $\omega = \sqrt{10/3}\,\omega_\perp$, whereas in a weakly collisional gas, $\omega = 2\omega_\perp$ (81, 82). The transition from ballistic behavior in the weak coupling limit to

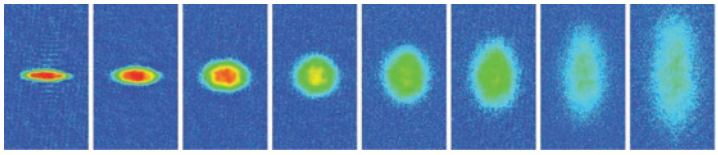

Figure 1

Expansion of a dilute Fermi gas at unitarity (78). The cloud contains $N \simeq 1.5 \times 10^5$ ^{6}Li atoms at a temperature $T = 8$ μK. Shown are a series of false-color absorption images taken between $t = 0.1$ and $t = 2.0$ ms. The scale of each image is the same. The axial size of the cloud remains nearly constant as the transverse size increases.

hydrodynamic behavior in the unitary gas has been observed experimentally (83, 84). In the hydrodynamic regime, damping of collective modes is governed by dissipative terms. The rate of energy dissipation is

$$\dot{E} = -\int \mathrm{d}^3x \left\{ \frac{1}{2}\eta(x)(\sigma_{ij})^2 + \zeta(x)\langle\sigma\rangle^2 + \frac{\kappa(x)}{T}(\nabla T)^2 \right\}. \qquad 32.$$

At unitarity, the system is scale invariant and the bulk viscosity is predicted to vanish (65, 85). This prediction has been experimentally verified (86). Thermal conductivity does not contribute to damping, because the gas is isothermal. As a consequence, the damping rate is a measure of shear viscosity.

Both the expansion and the collective-mode experiments involve approximate scaling flows. The motion is analogous to the Hubble flows in cosmology and to the Bjorken expansion of a QGP. Consider the Euler equation for the acceleration of an ideal fluid. We have $\dot{\boldsymbol{u}} \simeq -\nabla P/\rho = -\nabla\mu/m$, where we have used the Gibbs–Duhem relation $\mathrm{d}P = n\,\mathrm{d}\mu$. Because the external potential is harmonic, the chemical potential is harmonic, too. As a consequence, the velocity field is linear, and the cloud expands in a self-similar fashion. Because the fluid velocity is linear, the shear stress σ_{ij} is spatially constant and the rate of dissipation is sensitive to the spatial integral of $\eta(x)$:

$$\langle\eta\rangle = \int \mathrm{d}^3x\,\eta(x). \qquad 33.$$

Using measurements of the trap-integrated entropy, we can extract the ratio $\langle\eta\rangle/\langle s\rangle$. This analysis was originally performed in References 87 and 88. **Figure 2** shows a more recent analysis that combines collective-mode data at low T with expansion data at high T (80). The high-temperature data match expectations from kinetic theory. The viscosity drops with T, and the ratio of trap averages reaches $\langle\eta\rangle/\langle s\rangle \lesssim 0.4$.

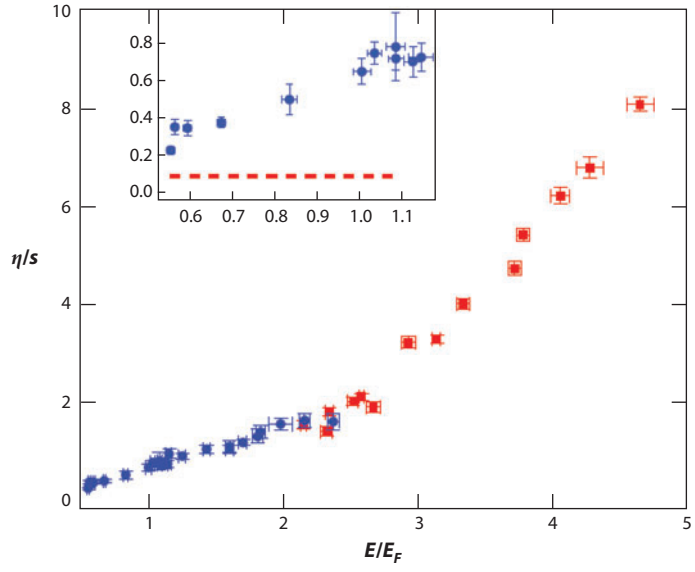

Figure 2

Measurements of η/s in the dilute Fermi gas at unitarity by use of collective modes (*blue circles*) and elliptic flow (*red squares*). Note that η/s in the plot refers to a ratio of trap integrated quantities, $\langle\eta\rangle/\langle s\rangle$. (*Inset*) The dashed line corresponds to the proposed bound $\eta/s = 1/(4\pi)$. Modified from Reference 80.

It is clearly desirable to unfold these measurements and determine local values of η/s. The main difficulty is a reliable treatment of the low-density corona. In this regime, η is independent of density and the integral in Equation 33 is ill defined, signaling the breakdown of fluid dynamics in the dilute region. The problem also appears if one applies the Navier–Stokes equation to an expanding gas cloud. In the dilute regime, η is not a function of density and the viscous stresses $\eta\sigma_{ij}$ are independent of position, implying that although ideal stresses propagate with the speed of sound, viscous stresses propagate with infinite speed. As discussed in Section 1.1, this problem can be solved by including a finite relaxation time (79, 89). In the low-density regime, the viscous relaxation time $\tau_R \simeq \eta/(nT)$ is large. Because the dissipative stresses are zero initially, taking a finite relaxation time into account suppresses the contribution of the corona. A schematic version of this idea was used by Cao et al. (80), but a more systematic treatment is needed.

3. RELATIVISTIC FLUIDS

3.1. The Quark–Gluon Plasma

The QGP is a hot, dense system of quarks and gluons governed by the QCD Lagrangian

$$\mathcal{L} = -\frac{1}{4}G^a_{\mu\nu}G^a_{\mu\nu} + \sum_f \bar{q}_f(i\gamma^\mu D_\mu - m_f)q_f, \qquad 34.$$

where $G^a_{\mu\nu} = \partial_\mu A^a_\nu - \partial_\nu A^a_\mu + g f^{abc} A^b_\mu A^c_\nu$ is the QCD field strength tensor, g is the coupling constant, and f^{abc} are the $SU(3)$ structure constants. The covariant derivative acting on the quark fields is $iD_\mu q = [i\partial_\mu + gA^a_\mu(\lambda^a/2)]q$, and m_f is the quark mass. At the temperature scale probed in RHIC or LHC experiments, the three light flavors (up, down, and strange) are thermally populated, whereas the heavy flavors (mainly charm and bottom) are produced in hard collisions and can serve as probes of the medium.

Asymptotic freedom implies that at very high temperature the QGP can be described in terms of quark and gluon quasi-particles. A typical gluon has a thermal momentum of order T. Soft gluons with momenta much lower than T are modified by interaction with hard particles. As a consequence, electric gluons acquire a Debye screening mass: $m_D \sim gT$. In perturbation theory there is no static screening of magnetic fields, but magnetic gluons are dynamically screened for momenta greater than $(m_D^2\omega)^{1/3}$, where ω is the frequency. The static magnetic sector of QCD is nonperturbative even if the temperature is very large. Confinement in three-dimensional pure gauge theory generates a mass scale of order g^2T. This mass scale determines the magnetic screening scale in the QGP: $m_M \sim g^2T$.

Perturbation theory in the QGP is based on the separation of scales: $m_M \ll m_D \ll T$. Strict perturbation theory in g works only for very low values of the coupling constant, $g \lesssim 1$ (90). However, quasi-particle models that rely on the separation of scales describe the thermodynamics of the plasma quite well, even for temperatures close to the phase transition to a hadronic gas (91).

The dispersion relation for the bosonic modes in the plasma evolves smoothly from quasi-gluons with masses $m \sim m_D$ at momenta $q \gtrsim gT$ to collective oscillations, plasmons, at low q. The energy of the plasmon in the limit $q \to 0$ is $\omega_P = m_D/\sqrt{3}$, and the plasmon width is $\Gamma \sim g^2T$ (92). The calculation of the collisional width of quasi-particles with momenta of order T is a complicated, nonperturbative problem, but the width remains parametrically small: $\Gamma \sim g^2\log(1/g)T$ (93).

Momentum diffusion is controlled by binary scattering between quarks and gluons. The cross section is proportional to g^4, and the IR divergence due to the exchange of massless gluons is regulated by dynamic screening. As a consequence, the shear viscosity scales as $\eta \sim T^3/[g^4\log(1/g)]$.

A detailed calculation in $N_f = 3$ QCD gives (94–96)

$$\eta = \frac{kT^3}{g^4 \log(\mu^*/m_D)}, \qquad 35.$$

where $k = 106.67$. The scale inside the logarithm is sensitive to bremsstrahlung processes such as $gg \to ggg$. Arnold et al. (95, 96) found $\mu^* = 2.96T$. The timescale for momentum diffusion is $\eta/(sT) \sim 1/[g^4 \log(1/g)T]$. This scale is parametrically large, but the precise value is very sensitive to the coupling constant. In $N_f = 3$ QCD, we get $\eta/s \simeq 9.2/[g^4 \log(1/g)]$. Using $g \simeq 2$ (which corresponds to $\alpha_s \simeq 0.3$) and $\log(1/g) \gtrsim 1$, we conclude that $\eta/s \lesssim 0.6$.

At $T \simeq 150$ MeV, the QGP undergoes a crossover transition to a hadronic resonance gas (97, 98). The resonance gas is strongly coupled, but as the temperature is reduced further, the system evolves to a weakly coupled gas of mostly pions, kaons, and nucleons. The viscosity of a pion gas is parametrically large: $\eta/s \sim (f_\pi/T)^4$, where $f_\pi \simeq 93$ MeV is the pion decay constant (99). Similar to the arguments in the case of cold Fermi gases, we therefore expect that η/s has a minimum in the vicinity of T_c. In this regime, the only reliable theoretical approach is lattice gauge theory. As in the case of nonrelativistic fermions, the calculations are difficult to perform because one has to extract the viscosity spectral function from imaginary time data. In the case of pure gauge theory, Meyer (30) finds $\eta/s = 0.102(56)$ at $T = 1.24T_c$ and $\eta/s = 34(33)$ at $T = 1.65T_c$.

Useful constraints on the spectral function are provided by sum rules. Romatschke & Son (100) showed that

$$\frac{2}{\pi} \int d\omega \, [\eta(\omega) - \eta_{T=0}(\omega)] = \frac{2}{5}\mathcal{E}, \qquad 36.$$

where $\eta_{T=0}(\omega)$ is the spectral function at zero temperature. The high-frequency behavior can be studied in perturbation theory. We find $\eta(\omega) \sim \omega^3$ at both zero and nonzero temperatures. Finite temperature effects were studied in References 101 and 102. We note that in nonrelativistic theories the tail of the spectral function is determined by short-range correlations, whereas in relativistic theories the high-frequency behavior is determined by the gg and $q\bar{q}$ continuum. In kinetic theory, the shape of the spectral function at low frequency is a Lorentzian with a width proportional to $1/\eta$. The lattice calculation in Reference 30 does not find a quasi-particle peak, but the resolution is insufficient to draw a final conclusions. A spectral function that is broadly consistent with the existence of quasi-particles was observed in a study of the electric conductivity of the QGP (103).

3.2. Flow, Higher Moments of Flow, and Viscosity

Experimental information about transport properties of the QGP comes from the observation of hydrodynamic flow in heavy-ion collisions at collider energies (104, 105). Several observations support the assumption that heavy-ion collisions create a locally thermalized system:

1. The overall abundances of produced particles is described by a simple thermal model that depends on only two parameters, the temperature T and the baryon chemical potential μ at freeze-out (106, 107).
2. For transverse momenta $p_\perp \lesssim 2$ GeV, the spectra dN/d^3p of produced particles follow a modified Boltzmann distribution characterized by the freeze-out temperature and a collective radial expansion velocity (104, 108). Radial flow manifests itself in the fact that the spectra of heavy hadrons, which acquire a larger momentum boost from the collective expansion, have a larger apparent temperature than the spectra of light hadrons.
3. In noncentral collisions, the azimuthal distribution of produced particles shows a strong anisotropy termed elliptic flow (104, 109). Elliptic flow represents the collective response of

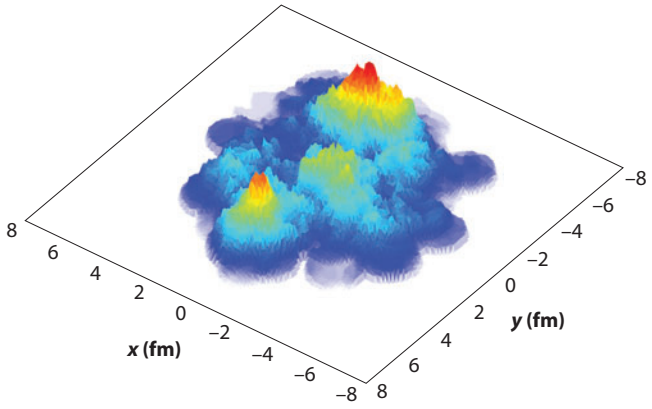

Figure 3

Initial energy density in an Au + Au collision at RHIC from the Monte Carlo KLN model (110, 111). This model includes the effects from the collision geometry, fluctuations in the initial position of the nucleons inside the nucleus, and nonlinear gluon field evolution. More sophisticated versions of the model also include quantum fluctuations of the gluon field.

the QGP to pressure gradients in the initial state, which in turn are related to the geometry of the overlap region of the colliding nuclei (**Figure 3**).

Analysis of the azimuthal distribution is the main tool for constraining the shear viscosity of the plasma. We define harmonics of the particle distribution

$$p_0 \frac{\mathrm{d}N}{\mathrm{d}^3 p}\bigg|_{p_z=0} = v_0(p_\mathrm{T})[1 + 2v_1(p_\mathrm{T})\cos(\phi - \Psi_1) + 2v_2(p_\mathrm{T})\cos(2\phi - \Psi_2) + \ldots], \qquad 37.$$

where p_z is the longitudinal (beam) direction, p_T is the transverse momentum, and ϕ is the angle relative to the impact parameter direction. The coefficient v_2 is known as elliptic flow, and the higher moments are known as, for example, triangular or quadrupolar flow. The angles Ψ_i are known as flow angles. Substantial elliptic flow, reaching approximately $v_2(p_\mathrm{T} = 2\,\mathrm{GeV}) \simeq 20\%$ in semicentral collisions, was discovered in the early RHIC data (112, 113) and confirmed at the LHC (114). More recently, studies found that fluctuations in the initial energy density generate substantial higher harmonics, including odd Fourier moments such as v_3 (115), and fluctuations of the flow angles relative to the impact parameter plane.

Viscosity tends to equalize the radial flow velocity and suppress elliptic flow and higher flow harmonics. An estimate of the relevant scales can be obtained from simple scaling solutions of fluid dynamics. The simplest solution of this type was proposed by Bjorken (118), who considered a purely longitudinal expansion. Bjorken assumed that the initial entropy density is independent of rapidity and that the subsequent evolution is invariant under boosts along the z axis. The Bjorken solution provides a natural starting point for more detailed numerical and analytical studies (104, 119). Bjorken flow is characterized by a flow profile of the form $u_\mu = \gamma(1, 0, 0, u_z) = (t/\tau, 0, 0, z/\tau)$, where $\gamma = (1 - u_z^2)^{1/2}$ is the boost factor and $\tau = (t^2 - z^2)^{1/2}$ is the proper time. This velocity field solves the relativistic Navier–Stokes equation. Energy conservation then determines the evolution of the entropy density. We find

$$-\frac{\tau}{s}\frac{\mathrm{d}s}{\mathrm{d}\tau} = 1 - \frac{4}{3}\frac{\eta}{sT\tau}, \qquad 38.$$

where we have neglected bulk viscosity. In ideal hydrodynamics, $s \sim T^3$ and $T \sim 1/\tau^{1/3}$. The validity of the gradient expansion requires that the viscous correction be small (5):

$$\frac{\eta}{s} \ll \frac{3}{4}(T\tau). \tag{39.}$$

It is usually assumed that in the QGP η/s is approximately constant. For the Bjorken solution, $T\tau \sim \tau^{2/3}$ increases with time, and Equation 39 is most restrictive during the early stages of the evolution. The use of an equilibration time $\tau_0 = 1$ fm and an initial temperature $T_0 = 300$ MeV gives $\eta/s \lesssim 0.6$. We conclude that fluid dynamics can be applied to heavy-ion collisions only if the QGP behaves as a nearly perfect fluid.

At late times, the expansion becomes three dimensional and $T\tau$ is independent of time. The fluid is composed of hadronic resonances that have cross sections that reflect hadronic sizes and are approximately independent of energy. In that case, $\eta \sim T/\sigma$. Using $s \sim T^3$ and $T \sim 1/\tau$, we find that the dissipative correction $\eta/(s\,T\,\tau)$ increases with proper time as τ^2. This result shows that fluid dynamics also breaks down at late times. At RHIC and LHC energies, the duration of the fluid dynamic phase is 5–10 fm/c, depending on collision energy and geometry. We note that, in contrast to the situation in heavy-ion collisions, there is no freeze-out in the cold atomic gas experiments. At unitarity the mean cross section increases as the temperature drops, and the fluid parameter $\eta/(nT\tau)$ is approximately constant during the evolution.

In heavy-ion collisions, we can observe only the final distribution of hadrons. In principle one could imagine reconstructing azimuthal harmonics of the stress tensor from the measured particle distribution, but doing so would require very complete coverage and particle identification, and it has not been attempted. In any case, hadrons continue to interact after the fluid freezes out, and some rearrangement of momentum takes place. This means that we need a prescription for converting hydrodynamic variables to kinetic distribution functions. What is usually done is that on the freeze-out surface the conserved densities in fluid dynamics are matched to kinetic theory (120).

In ideal fluid dynamics, the distribution functions are Bose–Einstein or Fermi–Dirac distributions characterized by the local temperature and fluid velocity. Viscosity modifies the stress tensor, and via matching to kinetic theory this modification changes the distribution functions f_p. The value of η/s constrains only the $p_i v_j$ moment of the distribution function. The full distribution function can be reconstructed only if the collision term is specified. Using the BGK collision term, one obtains a very simple formula for the leading correction δf_p:

$$\delta f_p = \frac{1}{2T^3}\frac{\eta}{s} f_0(1 \pm f_0) p_\alpha p_\beta \sigma^{\alpha\beta}, \tag{40.}$$

where the plus/minus sign refers to Bose/Fermi distributions, respectively. This result is a reasonable approximation to more microscopic theories (95). The shift in the distribution function leads to a modification of the single-particle spectrum. In the case of the Bjorken expansion and at large p_T, we find

$$\frac{\delta(dN)}{dN_0} = \frac{1}{3\tau_f T_f}\frac{\eta}{s}\left(\frac{p_T}{T_f}\right)^2, \tag{41.}$$

where dN_0 is the number of particles produced in ideal fluid dynamics, $\delta(dN)$ is the dissipative correction, and τ_f is the freeze-out time. In a system with strong longitudinal expansion, viscous corrections tend to equalize the momentum flow by pushing particles to higher p_T. Because the single-particle distribution enters into the denominator of v_2, this effect tends to suppress v_2 at large p_T. The effect from the numerator, dissipative corrections due to the $\cos(2\phi)$ component

of the radial flow, acts in the same direction (121). What is important is that corrections to the spectrum are controlled by the same parameter $\eta/(s\tau T)$ that governs the derivative expansion in fluid dynamics. This reflects that in the regime in which kinetic theory can be matched to fluid dynamics we have $\mathrm{Kn} \sim \mathrm{Re}^{-1}$.

We obtain several simple predictions that have been confirmed by experiment (122): Dissipative corrections increase with p_T, they are larger in small systems that freeze out earlier, and they are larger for higher harmonics that are more sensitive to gradients of the radial flow profile. Quantitative predictions that provide not only bounds on η/s but also reliable measurements of transport properties of the plasma require a number of ingredients (123):

1. An initial-state model that incorporates the nuclear geometry and fluctuations in the initial energy deposition. The simplest possibility is a Monte Carlo implementation of the Glauber model (124), but some calculations also include saturation effects, quantum fluctuations of the initial color field, and preequilibrium evolution of the initial field (117). Alternatively, one may try to describe the preequilibrium stage by using kinetic theory (125, 126) or the AdS/CFT correspondence (127). At the end of the initial stage, the stress tensor is matched to fluid dynamics.
2. Second-order dissipative fluid dynamics in 2+1 (boost-invariant) or 3+1 dimensions. Calculations must include checks to ensure insensitivity to poorly constrained second-order transport coefficients and a realistic equation of state. A realistic equation of state has to match lattice QCD results at high temperature and a hadronic resonance gas below T_c (128). The resonance gas equation of state must allow for chemical nonequilibrium effects below the chemical freeze-out temperature, $T_{\mathrm{chem}} \simeq T_c$.
3. Kinetic freeze-out and a kinetic afterburner. At the kinetic freeze-out temperature, the fluid is converted to hadronic distribution functions. Ideally, these distribution functions are evolved further using a hadronic cascade (129, 130), but at a minimum one has to include feed-down from hadronic resonance decays.

Initial estimates of η/s from the RHIC data have been obtained (131–133). **Figure 4** shows a more recent analysis of LHC data (117). The authors found $\eta/s \simeq 0.2$ at the LHC and $\eta/s \simeq 0.12$ from a similar analysis of RHIC data. Similar results were obtained by other authors. Song et al. (134) reported an average value of $\eta/s \simeq (0.2\text{-}0.24)$ at the LHC and $\eta/s \simeq 0.16$ at RHIC. Luzum & Ollitrault (135) tried to constrain the allowed range of η/s, obtaining $0.07 \leq \eta/s \leq 0.43$ at RHIC. Given the complexity of the analysis, uncertainties are difficult to quantify. A survey of the main sources of error in the determination of η/s can be found in Reference 136. Interestingly, the extracted values of η/s are lower at RHIC than they are at the LHC, as one would expect on the basis of asymptotic freedom. We emphasize, however, that given the uncertainties it is too early to make this statement with high confidence.

4. FRONTIERS

In absolute units, the shear viscosity of the ultracold Fermi gas and that of the QGP differ by more than 25 orders of magnitude (7). The approximate universality of η/s in strongly coupled fluids, and the near agreement with the value predicted by the AdS/CFT correspondence in the strong coupling limit of a large class of field theories, is quite remarkable. Much work remains to be done to determine to what extent this observation can be made precise and what it implies about the structure of strongly correlated quantum systems. In this outlook, we can provide only a very brief summary of some of these issues.

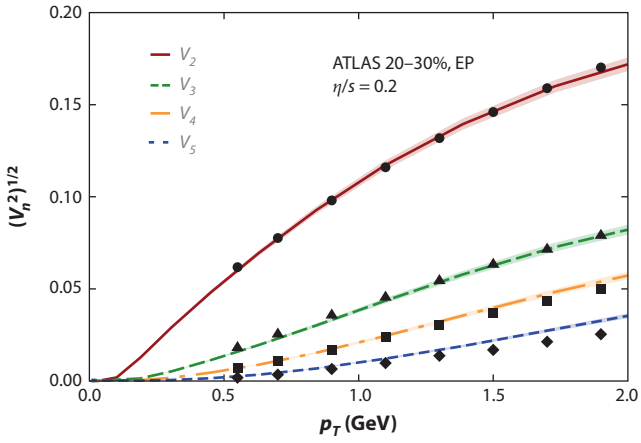

Figure 4

Fourier coefficients $v_2, \ldots, v_5$ of the azimuthal charged-particle distribution as a function of the transverse momentum p_T measured in Pb + Pb collisions at the LHC (116). The measurements were performed using the event plane (EP) method and correspond to the 20–30% centrality class. The dashed lines represent a hydrodynamic analysis performed with $\eta/s = 0.2$ (117).

4.1. Transport Coefficients

There is an ongoing effort to map out the full density and temperature dependence of η/s in both the ultracold gases and the QGP and to determine other transport coefficients, such as the bulk viscosity and diffusion coefficients. Several experimental puzzles remain to be addressed. In the case of heavy-ion collisions, nearly ideal flow is even more pervasive than one would expect. Strong flow is also observed in photons, electrons from heavy-quark decays, and hadrons emitted in high-multiplicity p + Pb collisions at LHC energies; see Reference 137 for a recent summary and original references. In the case of cold atomic gases, we now have very accurate data for the dependence of $\langle\eta\rangle$ on the total energy of the cloud (138). These data have not been unfolded. It was observed that the scaling of $\langle\eta\rangle$ with the total energy is remarkably simple—$\langle\eta\rangle/\langle n\rangle \sim aE + bE^3$ for all energies above the critical point—but the origin of this scaling behavior is not understood.

4.2. Quasi-Particles

We would like to understand whether nearly perfect fluidity, $\eta/s \sim 1/(4\pi)$, necessarily implies the absence of quasi-particles, as is the case in the AdS/CFT correspondence. The most direct way to study this issue is to determine the spectral function. Because the only local probe of the stress tensor is the graviton, this task will probably require numerical studies. We are also interested in pushing weak coupling descriptions into the regime where the quasi-particle picture breaks down, for example, by using the renormalization group.

4.3. Viscosity Bound

Whether there is a fundamental lower limit for η/s is unknown. Part of the issue may well be that we need to define more carefully what we mean by a fluid, and that we need to understand how these defining characteristics are reflected in microscopic theories. We would also like to know what kinds of theories have holographic duals and what aspects of the field theory lead to the emergence of certain universal features, such as the strong coupling limit $\eta/s = 1/(4\pi)$.

4.4. Other Strongly Correlated Fluids

In addition to the two fluids discussed in this review, several other systems may be of interest. One interesting class consists of two-dimensional fluids, for example, the electron gas in graphene (139) and the so-called strange metal phase of the high-T_c superconductors (140).

4.5. Equilibration at Strong and Weak Coupling

Empirical evidence suggests that equilibration in heavy-ion collisions takes place on a very short timescale: $\tau_{eq} \sim 1$ fm. Rapid equilibration is natural in holographic theories (46), but it is difficult to make contact with asymptotic freedom and the well-established theory and phenomenology of parton distribution functions. Understanding equilibration in weak coupling is a complicated problem that involves many competing scales, and even establishing the parametric dependence of the equilibration time on α_s is difficult; see Reference 141 for a recent overview.

4.6. Anomalous Hydrodynamics

Several novel hydrodynamic effects have been discovered in recent years. An example is the chiral magnetic effect. Topological charge fluctuations in the initial state of a heavy-ion collision, combined with the magnetic field generated by the highly charged ions, can manifest themselves in electric-charge fluctuations in the final state (142). This effect is now understood as part of a broader class of anomalous hydrodynamic effects (143). Anomalous transport coefficients were originally discovered in the context of holographic dualities (144) and interpreted using general arguments based on fluid dynamics (145).

DISCLOSURE STATEMENT

The author is not aware of any affiliations, memberships, funding, or financial holdings that might be perceived as affecting the objectivity of this review.

ACKNOWLEDGMENTS

My work was supported in part by the US Department of Energy grant DE-FG02-03ER41260. I acknowledge useful discussions with Peter Arnold, Dam Son, Derek Teaney, and John Thomas.

LITERATURE CITED

1. Kadanoff LP, Martin PC. *Ann. Phys.* 24:419 (1963)
2. Forster D. *Hydrodynamic Fluctuations, Broken Symmetry, and Correlation Functions*. New York: Addison Wesley (1995)
3. Reiner M. *Phys. Today* 17:62 (1964)
4. Purcell EM. *Am. J. Phys.* 45:3 (1977)
5. Danielewicz P, Gyulassy M. *Phys. Rev. D* 31:53 (1985)
6. Kovtun P, Son DT, Starinets AO. *Phys. Rev. Lett.* 94:111601 (2005)
7. Schäfer T, Teaney D. *Rep. Prog. Phys.* 72:126001 (2009)
8. Adams A, et al. *New J. Phys.* 14:115009 (2012)
9. Burnett D. *Proc. Lond. Math. Soc.* 39:385 (1935)
10. Garcia-Colina LS, Velascoa RM, Uribea FJ. *Phys. Rep.* 465:149 (2008)
11. Grad H. *Commun. Pure Appl. Math.* 2:331 (1949)
12. Israel W, Stewart JM. *Ann. Phys.* 118:341 (1979)

13. Romatschke P. *Int. J. Mod. Phys. E* 19:1 (2010)
14. Cattaneo C. *Atti Sem. Mat. Fis. Univ. Modena* 3:3 (1948)
15. Müller I. *A History of Thermodynamics*. Heidelberg, Ger.: Springer (2006)
16. Müller I. *Z. Phys.* 198:329 (1967)
17. Israel W, Stewart JM. *Phys. Lett. A* 58:213 (1967)
18. Baier R, et al. *J. High Energy Phys.* 0804:100 (2008)
19. Chao J, Schäfer T. *Ann. Phys.* 327:1852 (2012)
20. Kovtun P, Moore GD, Romatschke P. *Phys. Rev. D* 84:025006 (2011)
21. Chafin C, Schäfer T. *Phys. Rev. A* 87:023629 (2013)
22. Adhikari R, Cates ME, Stratford K, Wagner AJ. *Europhys. Lett.* 71:473 (2005)
23. Murase K, Hirano T. arXiv:1304.3243 [nucl-th] (2013)
24. Bhatnagar PL, Gross EP, Krook M. *Phys. Rev.* 94:511 (1954)
25. Chapman S, Cowling TG. *The Mathematical Theory of Non-Uniform Gases*. Cambridge, UK: Cambridge Univ. Press. 3rd ed. (1970)
26. Kadanoff LP, Baym G. *Quantum Statistical Mechanics: Green's Function Methods in Equilibrium and Nonequilibrium Problems*. New York: Benjamin (1962)
27. Maxwell JC, Garber E, Brush SG, Everitt CWF. *Maxwell on Molecules and Gases*. Cambridge, MA: MIT Press (1986)
28. Brush SG. *The Kind of Motion We Call Heat*. Amsterdam: North-Holland (1986)
29. Karsch F, Wyld HW. *Phys. Rev. D* 35:2518 (1987)
30. Meyer HB. *Phys. Rev. D* 76:101701 (2007)
31. Sakai S, Nakamura A. *Proc. Sci.* LAT2007:221 (2007)
32. Aarts G, et al. *Phys. Rev. Lett.* 99:022002 (2007)
33. Meyer HB. *Eur. Phys. J. A* 47:86 (2011)
34. Wlazlowski G, Magierski P, Bulgac A, Roche KJ. *Phys. Rev. A* 013639:88 (2013)
35. Thorne KS, Price RH, MacDonald DA. *Black Holes: The Membrane Paradigm*. New Haven, CT: Yale Univ. Press (1986)
36. Maldacena JM. *Adv. Theor. Math. Phys.* 2:231 (1998)
37. Son DT, Starinets AO. *Annu. Rev. Nucl. Part. Sci.* 57:95 (2007)
38. Gubser SS, Karch A. *Annu. Rev. Nucl. Part. Sci.* 59:145 (2009)
39. Casalderrey-Solana J, et al. arXiv:1101.0618 [hep-th] (2011)
40. DeWolfe O, Gubser SS, Rosen C, Teaney D. arXiv:1304.7794 [hep-th] (2013)
41. Policastro G, Son DT, Starinets AO. *J. High Energy Phys.* 0209:043 (2002)
42. Teaney D. *Phys. Rev. D* 74:045025 (2006)
43. Policastro G, Son DT, Starinets AO. *Phys. Rev. Lett.* 87:081601 (2001)
44. Kovtun PK, Starinets AO. *Phys. Rev. Lett.* 96:131601 (2006)
45. Kovtun PK, Starinets AO. *Phys. Rev. D* 72:086009 (2005)
46. Chesler PM, Yaffe LG. *Phys. Rev. Lett.* 106:021601 (2011)
47. Heller MP, Janik RA, Witaszczyk P. *Phys. Rev. Lett.* 108:201602 (2012)
48. Heller MP, Janik RA, Witaszczyk P. *Phys. Rev. Lett.* 110:211602 (2013)
49. Kovtun P, Yaffe LG. *Phys. Rev. D* 68:025007 (2003)
50. Bhattacharyya S, Hubeny VE, Minwalla S, Rangamani M. *J. High Energy Phys.* 0802:045 (2008)
51. Rangamani M. *Class. Quantum Gravity* 26:224003 (2009)
52. Cohen TD. *Phys. Rev. Lett.* 99:021602 (2007)
53. Mott NF. *Philos. Mag.* 26:1015 (1972)
54. Paalanen MA, Rosenbaum TF, Thomas GA, Bhatt RN. *Phys. Rev. Lett.* 48:1284 (1982)
55. Buchel A, Liu JT. *Phys. Rev. Lett.* 93:090602 (2004)
56. Iqbal N, Liu H. *Phys. Rev. D* 79:025023 (2009)
57. Herzog CP, et al. *J. High Energy Phys.* 0607:013 (2006)
58. Casalderrey-Solana J, Teaney D. *Phys. Rev. D* 74:085012 (2006)
59. Gubser SS. *Phys. Rev. D* 74:126005 (2006)
60. Kats Y, Petrov P. *J. High Energy Phys.* 0901:044 (2009)
61. Cremonini S. *Mod. Phys. Lett. B* 25:1867 (2011)

62. Brigante M, et al. *Phys. Rev. D* 77:126006 (2008)
63. Buchel A, Myers RC. *J. High Energy Phys.* 0908:016 (2009)
64. Camanho XO, Edelstein JD, Paulos MF. *J. High Energy Phys.* 1105:127 (2011)
65. Castin Y, Werner F. arXiv:1103.2851v2 [cond-mat.quant-gas] (2011)
66. Bloch I, Dalibard J, Zwerger W. *Rev. Mod. Phys.* 80:885 (2008)
67. Giorgini S, Pitaevskii LP, Stringari S. *Rev. Mod. Phys.* 80:1215 (2008)
68. Schäfer T, Dusling K. *Phys. Rev. Lett.* 111:120603 (2013)
69. Massignan P, Bruun GM, Smith H. *Phys. Rev. A* 71:033607 (2005)
70. Bruun GM, Smith H. *Phys. Rev. A* 72:043605 (2005)
71. Ku MJH, Sommer AT, Cheuk LW, Zwierlein MW. *Science* 335:563 (2012)
72. Rupak G, Schäfer T. *Phys. Rev. A* 76:053607 (2007)
73. Enss T, Haussmann R, Zwerger W. *Ann. Phys.* 326:770 (2011)
74. Braby M, Chao J, Schäfer T. *New J. Phys.* 13:035014 (2011)
75. Taylor E, Randeria M. *Phys. Rev. A* 81:053610 (2010)
76. Tan S. *Ann. Phys.* 323:2971 (2008)
77. Hofmann J. *Phys. Rev. A* 84:043603 (2011)
78. O'Hara KM, et al. *Science* 298:2179 (2002)
79. Schäfer T, Chafin C. *Lect. Notes Phys.* 836:375 (2012)
80. Cao C, et al. *Science* 331:58 (2011)
81. Stringari S. *Europhys. Lett.* 65:749 (2004)
82. Bulgac A, Bertsch GF. *Phys. Rev. Lett.* 94:070401 (2005)
83. Kinast J, Turlapov A, Thomas JE. *Phys. Rev. A* 70:051401(R) (2004)
84. Bartenstein M, et al. *Phys. Rev. Lett.* 92:203201 (2004)
85. Son DT. *Phys. Rev. Lett.* 98:020604 (2007)
86. Elliott E, Joseph JA, Thomas JE. arXiv:1308.3162 [cond-mat.quant-gas] (2013)
87. Schäfer T. *Phys. Rev. A* 76:063618 (2007)
88. Turlapov A. *J. Low Temp. Phys.* 150:567 (2008)
89. Bruun GM, Smith H. *Phys. Rev. A* 76:045602 (2007)
90. Kajantie K, Laine M, Rummukainen K, Schröder Y. *Phys. Rev. D* 67:105008 (2003)
91. Blaizot JP, Iancu E, Rebhan A. In *Quark Gluon Plasma 3*, ed. R Hwa, X-N Wang, p. 60. Singapore: World Sci. (2003)
92. Braaten E, Pisarski RD. *Phys. Rev. D* 42:2156 (1990)
93. Blaizot JP, Iancu E. *Nucl. Phys. B* 570:326 (2000)
94. Baym G, Monien H, Pethick CJ, Ravenhall DG. *Phys. Rev. Lett.* 64:1867 (1990)
95. Arnold P, Moore GD, Yaffe LG. *J. High Energy Phys.* 0011:001 (2000)
96. Arnold P, Moore GD, Yaffe LG. *J. High Energy Phys.* 0305:051 (2003)
97. Aoki Y, Fodor Z, Katz SD, Szabo KK. *Phys. Lett. B* 643:46 (2006)
98. Bazavov A, et al. *Phys. Rev. D* 85:054503 (2012)
99. Prakash M, Prakash M, Venugopalan R, Welke G. *Phys. Rep.* 227:321 (1993)
100. Romatschke P, Son DT. *Phys. Rev. D* 80:065021 (2009)
101. Aarts G, Martinez Resco JM. *J. High Energy Phys.* 0204:053 (2002)
102. Zhu Y, Vuorinen A. *J. High Energy Phys.* 1303:002 (2013)
103. Ding HT, et al. *Phys. Rev. D* 83:034504 (2011)
104. Heinz UW. arXiv:0901.4355 [nucl-th] (2009)
105. Teaney DA. arXiv:0905.2433 [nucl-th] (2009)
106. Cleymans J, Satz H. *Z. Phys. C* 57:135 (1993)
107. Braun-Munzinger P, Wambach J. *Rev. Mod. Phys.* 81:1031 (2009)
108. Schnedermann E, Sollfrank J, Heinz UW. *Phys. Rev. C* 48:2462 (1993)
109. Ollitrault J-Y. *Phys. Rev. D* 46:229 (1992)
110. Schenke B, Tribedy P, Venugopalan R. *Phys. Rev. Lett.* 108:252301 (2012)
111. Kharzeev D, Nardi M. *Phys. Lett. B* 507:121 (2011)
112. Adler SS, et al. (PHENIX Collab.) *Phys. Rev. Lett.* 91:182301 (2003)
113. Adams J, et al. (STAR Collab.) *Phys. Rev. C* 72:014904 (2005)

114. Aamodt K, et al. (ALICE Collab.) *Phys. Rev. Lett.* 105:252302 (2010)
115. Alver B, Roland G. *Phys. Rev. C* 81:054905 (2010)
116. Aad G, et al. (ATLAS Collab.) *Phys. Rev. C* 86:014907 (2012)
117. Gale C, et al. *Phys. Rev. Lett.* 110:012302 (2013)
118. Bjorken JD. *Phys. Rev. D* 27:140 (1983)
119. Gubser SS, Yarom A. *Nucl. Phys. B* 846:469 (2011)
120. Cooper F, Frye G. *Phys. Rev. D* 10:186 (1974)
121. Teaney D. *Phys. Rev. C* 68:034913 (2003)
122. Heinz U, Snellings R. *Annu. Rev. Nucl. Part. Sci.* 63:123 (2013)
123. Gale C, Jeon S, Schenke B. *Int. J. Mod. Phys. A* 28:1340011 (2013)
124. Miller ML, Reygers K, Sanders SJ, Steinberg P. *Annu. Rev. Nucl. Part. Sci.* 57:205 (2007)
125. Martinez M, Strickland M. *Nucl. Phys. A* 848:183 (2010)
126. Petersen H, et al. *Phys. Rev. C* 78:044901 (2008)
127. van der Schee W, Romatschke P, Pratt S. *Phys. Rev. Lett.* 111:222302 (2013)
128. Huovinen P, Petreczky P. *Nucl. Phys. A* 837:26 (2010)
129. Bass SA, Dumitru A. *Phys. Rev. C* 61:064909 (2000)
130. Hirano T, et al. *Phys. Lett. B* 636:299 (2006)
131. Romatschke P, Romatschke U. *Phys. Rev. Lett.* 99:172301 (2007)
132. Dusling K, Teaney D. *Phys. Rev. C* 77:034905 (2008)
133. Song H, Heinz UW. *Phys. Rev. C* 77:064901 (2008)
134. Song H, Bass SA, Heinz U. *Phys. Rev. C* 83:054912 (2011); Song H, Bass SA, Heinz U. Erratum. *Phys. Rev. C* 87:019902 (2013)
135. Luzum M, Ollitrault J-Y. *Nucl. Phys. A* 904/905:377c (2013)
136. Song H, Heinz UW. *J. Phys. G* 36:064033 (2009)
137. Huovinen P. *Int. J. Mod. Phys. E* 22:1330029 (2013)
138. Elliott E, Joseph JA, Thomas JE. arXiv:1311.2049 [cond-mat.quant-gas] (2013)
139. Müller M, Schmalian J, Fritz L. *Phys. Rev. Lett.* 103:025301 (2009)
140. Guo H, Wulin D, Chien C-C, Levin K. *New J. Phys.* 13:075011 (2011)
141. Kurkela A, Moore GD. *J. High Energy Phys.* 1112:044 (2011)
142. Kharzeev DE, McLerran LD, Warringa HJ. *Nucl. Phys. A* 803:227 (2008)
143. Kharzeev DE, Son DT. *Phys. Rev. Lett.* 106:062301 (2011)
144. Erdmenger J, Haack M, Kaminski M, Yarom A. *J. High Energy Phys.* 0901:055 (2009)
145. Son DT, Surowka P. *Phys. Rev. Lett.* 103:191601 (2009)

Annual Review of Nuclear and Particle Science

Volume 64, 2014

Contents

Index

Errata

An online log of corrections to *Annual Review of Nuclear and Particle Science* articles may be found at http://www.annualreviews.org/errata/nucl